Immersed boundary modelling of cochlear mechanics

by

Fatemeh Saghafifar

B.Sc., Sharif University of Technology, 2018

Thesis Submitted in Partial Fulfillment of the
Requirements for the Degree of
Master of Science

in the
Department of Mathematics
Faculty of Science

© Fatemeh Saghafifar 2022
SIMON FRASER UNIVERSITY
Spring 2022

Declaration of Committee

Name: **Fatemeh Saghafifar**

Degree: **Master of Science**

Thesis title: **Immersed boundary modelling of cochlear mechanics**

Committee: **Chair:**   Paul Tupper
                                    Professor, Mathematics

                              John Stockie
                              Supervisor
                              Professor, Mathematics

                              Steven Ruuth
                              Committee Member
                              Professor, Mathematics

                              JF Williams
                              Examiner
                              Associate Professor, Mathematics

Abstract

The immersed boundary method (IBM) simulates the interaction between a flexible elastic structure and a surrounding incompressible fluid in which it is immersed. This method is particularly useful in modelling biological phenomena, ranging from human organ systems to the swaying seagrass on the sea bottom. One fascinating application of immersed boundaries is the study of fluid mechanics within the cochlea or inner ear, which transforms external sound waves into electrical impulses that are transmitted to the brain. An integral component of the cochlea is a flexible structure called the basilar membrane (BM) which is excited by oscillatory fluid motions induced within the cochlear duct. We implement a 2D immersed boundary model for the cochlea and study the BM oscillations that arise due to periodic forcing over a variety of frequencies that cover a subset of the range of human hearing. The results are compared with other model simulations.

Keywords: Immersed boundary method, fluid-structure interaction, cochlear mechanics, basilar membrane

Table of Contents

List of Figures

Chapter 1

Introduction

Nature is full of examples of fluid-structure interaction (FSI) problems in which a fluid comes in contact a solid or deformable structure and interacts with it. FSI problems occurs at different scales in biological settings, from cell scale problems to larger ones, such as blood flow in the heart. One interesting category of FSI problems is systems where a deformable elastic structure is immersed in a viscous incompressible fluid. This phenomenon is common in biofluid systems such as red blood cells deforming in a capillary, or seagrass that sways in response to ocean currents [32, 26]. Mathematical modelling is a useful tool to better understand these type of interactions.

In computational fluid dynamics, different methods can be used to describe the motion of a fluid interacting with the mentioned elastic structures. One of these methods that has demonstrated good performance for complicated FSI problems is called the immersed boundary method (IBM) [43]. This method was first introduced by Charles Peskin to study blood flow around valve leaflets of the heart [42] and has been used since to model many different biological phenomena. Another application of the immersed boundary method is the model introduced by Rejniak [51] for the growth of individual cells. Rejniak used this method to show how a single cell grows and divides. When they are fed, these cells proliferate and form a tumor. One other example of the IBM in bio-fluid problems is the study of the swimming dynamics of different organisms. For instance, Cortez *et al.* modelled the interaction of internal molecular motor mechanisms of beating cilia and flagella with a fluid using immersed boundary method [12].

In the mathematical formulation of the IBM, a combination of Lagrangian and Eulerian variables are used to represent the spatial discretization of the flexible structure and the fluid. The interaction between quantities on the Eulerian and Lagrangian grids is facilitated by: (1) spreading the IB forces onto the fluid grid, and (2) interpolating the fluid velocity onto the IB. Both spreading and interpolation operations are specified in terms of convolutions with Dirac delta functions. This method also incorporates a numerical scheme where the Eulerian variables are defined on a fixed Cartesian mesh and the deformable immersed boundary is parameterized using Lagrangian points that can move freely through

the Eulerian mesh. For the numerical implementation of the interaction equations, a smooth approximation of the Dirac delta function is employed [43].

The standard immersed boundary framework [43] is used in different implementations of this method. One example is this implementations is IBIS [15] which is developed in FORTRAN. IBAMR, an adaptive and parallel implementation of IB developed by Griffith [20], is another package which dynamically adapts the mesh size for higher resolution near critical areas. This software is written in C++ and it is very efficient for highly complicated 3D problems. However, installation and utilization of this software is not easy and requires a high level of programming experience. IB2d [7, 6] on the other hand, is a 2D implementation of this method implemented in both MATLAB and Python, which follows Peskin's framework and incorporates different choices of fiber models to connect the Lagrangian grids. It also includes a wide variety of examples in order to illustrate its applicability to a wide range of problems and make it easy for a new user to apply the code to study a new application. In this package, the user can construct the geometry and assign the suitable fibers and modify different parameters to better model an immersed boundary problem. Compared to IBAMR and IBIS, IB2d provides the tools to implement different 2D immersed boundary problems in a user-friendly environment. Other open source IB codes are also available, but they do not include the wide range of fiber force models and examples that IB2d does, which makes IB2d an ideal platform with which to implement a new problem [61, 37].

This thesis will focus on studying fluid-structure interactions that take place within the cochlea, which is one of the key elements in mammalian hearing systems. The main function of this organ, which is part of the inner ear, is to transduce the sounds entering the ear into some electrical impulses that the brain can understand. Scientists have been studying cochlear mechanics for almost a century, starting with the pioneering work of von Békésy in 1928 [58], who proposed a traveling wave theory for propagation of sound waves within the cochlea. This has been expanded on in a major way by other notable people like Gold [19], who was an experimentalist, and Lighthill [33], who was the first mathematician to study cochlear behavior. Allen and Neely [4] explained the cochlear mechanics in a readable manner for non-experts. Steele *et al.* [54] provided a recent review of different types of passive and active cochlea models. Finally, the work of Champneys *et al.* [11] and Keener and Sneyd [23] both provided in-depth summaries of the various mathematical models that have been applied to study cochlear mechanics.

Another interesting approach for modelling the cochlea is the immersed boundary method. FSI in the cochlea consists of the interaction between the perilymphatic fluid that fills the cochlear duct and a flexible membrane that runs down its center, known as the basilar membrane. The first two dimensional IB model of cochlea was introduced by LeVeque, Peskin and Lax [31], in which they provided both numerical and asymptotic results that approximate the cochlear dynamics. Following their work, Beyer [8] developed a 2D model in which the cochlea is represented as two fluid chambers separated by an elastic membrane.

His model simplifies the cochlea while maintaining the key features of it, leading to results comparable with the asymptotic results of LeVeque, Peskin and Lax.

In this thesis, we presented a 2D immersed boundary model of the cochlea based on the work by Beyer [8] using the IBM scheme developed by Peskin [43] and implemented in the IB2d package [7, 6]. We demonstrate that the IB model is capable of reproducing BM behavior observed in experiments as well as other numerical simulations.

Chapter 2

Immersed boundary method

The immersed boundary method introduced by Peskin [42, 43] for fluid-structure interaction problems is both a mathematical model and a numerical scheme. The model can be separated into three components: fluid motion equations, interaction equations and immersed boundary force equations. The fluid variables are represented at Euler grid points and the IB quantities at Lagrangian points as illustrated in Figure 2.1.

- Fluid motion equations: The fluid dynamics of many bio-fluid problems is governed by the incompressible Navier-Stokes equations:

$$\rho \left(\frac{\partial u}{\partial t} + \vec{u} \cdot \nabla \vec{u} \right) + \nabla p = \mu \Delta \vec{u} + \vec{f}, \tag{2.1}$$

$$\nabla \cdot \vec{u} = 0 \qquad \text{for } \vec{x} \in \Omega, \tag{2.2}$$

where $\vec{u}(\vec{x}, t)$ is the fluid velocity, $p(\vec{x}, t)$ is the pressure and $\vec{f}(\vec{x}, t)$ is the external force per unit area in 2D (or force per unit volume in 3D). Density and viscosity are constant and the fluid domain Ω is a subset of $\mathbb{R}^2$ or $\mathbb{R}^3$. These equations can be solved using standard fluid solvers.

- Interaction equations: The interaction between fluid and IB can be modeled as follows:

$$\vec{f}(\vec{x}, t) = \int_\Gamma \vec{F}(s, t) \delta(\vec{x} - \vec{X}(s)) ds, \tag{2.3}$$

$$\frac{\partial \vec{X}}{\partial t}(s, t) = \int_\Omega \vec{u}(\vec{x}, t) \delta(\vec{x} - \vec{X}(s)) d\vec{x}, \tag{2.4}$$

where $\vec{X}(s, t) \in \Gamma$ is the position of the elastic structure and s is is a Lagrangian coordinate that parameterizes the immersed boundary. Equation (2.3) shows how the force from IB deformations is spread onto fluid grid points through the Dirac delta function and equation (2.4) acts to interpolate the fluid velocity onto adjacent IB grid points. The 2D Dirac delta function is assumed to be separable into a product of two
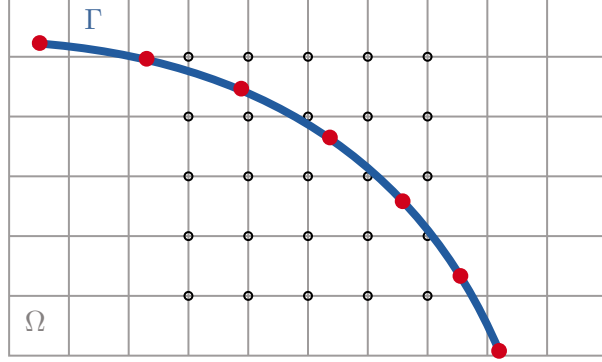
Figure 2.1: Schematic diagram of IBM discretization: Eulerian grid points (black nodes) discretizing the fluid domain Ω and Lagrangian points (red nodes) discretizing the immersed boundary Γ which is the blue curve.

1D delta functions:

$$\delta(\vec{x}) = \delta(x)\delta(y).$$

- Immersed boundary force equations: The deformable elastic nature of the immersed boundary is captured by treating it as a combination of individual 1D fibers, parameterized by s. The force density $F(s,t)$ is a functional of the current immersed boundary's configuration which can be defined as

$$\vec{F}(s,t) = \mathbb{F}(\vec{X}(s,t),t), \tag{2.5}$$

where $\mathbb{F}(\vec{X}(s,t),t)$ is a combination of all the fiber components modeling the desired material properties of the immersed structure.

Equations (2.1)-(2.5) make up the IBM framework introduced by Peskin. In the IB2d package, Battista [7] implements this scheme for 2D problems and introduces different fibers to represent the elastic structure.

2.1 Spatial discretization

Our numerical implementation of the IBM is formulated using the same spatial and temporal discretization as introduced in Peskin [43]. We start by describing the spatial discretization in 2D and assume that $\{\vec{e_1}, \vec{e_2}\}$ are the standard basis of $\mathbb{R}^2$, ϕ is a scalar function and $\vec{u}$ is a vector function. The central difference operator in each direction $\alpha = 1, 2$ is then defined as:

$$(D_\alpha \phi)(\vec{x}) = \frac{\phi(\vec{x} + h\vec{e_\alpha}) - \phi(\vec{x} - h\vec{e_\alpha})}{2h}. \tag{2.6}$$

where $\vec{x}$ is used in this section to refer to discrete points $\vec{x}_{ij} = (i\Delta x, j\Delta y)$ on an $N \times N$ fluid grid with $i, j = 1, \ldots, N$. However, we will suppress the subscripts i, j for simplicity of notation.

Based on this definition, we can write the discrete gradient and divergence operators as

$$\vec{D} = (D_1, D_2), \tag{2.7}$$

$$\vec{D}\phi = (D_1\phi, D_2\phi) \approx \nabla\phi, \tag{2.8}$$

$$\vec{D} \cdot \vec{u} = D_1 u_1 + D_2 u_2 \approx \nabla \cdot \vec{u}. \tag{2.9}$$

For the Laplacian that appears in the viscous term, we have:

$$(L\vec{u})(\vec{x}) = \sum_{\alpha=1}^{2} \frac{\vec{u}(\vec{x} + h\vec{e}_\alpha) + \vec{u}(\vec{x} - h\vec{e}_\alpha) - 2\vec{u}(\vec{x})}{h^2} \approx \Delta\vec{u}. \tag{2.10}$$

Finally, we want to discretize the nonlinear advetion term. Because $\nabla \cdot \vec{u} = 0$, we have

$$\vec{u} \cdot \nabla\phi = \nabla \cdot (\vec{u}\phi). \tag{2.11}$$

where ϕ is a scalar representing the velocity in each direction. While continuously this equality holds, the two terms will not always be equal discretely. That is why current scheme chooses the discretization of the nonlinear term to be the average of the discrezations of these two terms which is

$$S(\vec{u})\phi = \frac{1}{2}\vec{u} \cdot \vec{D}\phi + \frac{1}{2}\vec{D}(\vec{u}\phi), \tag{2.12}$$

This operator ends up being skew-symmetric, which means $S^T = -S$ (proof provided by Peskin [43]). The important feature of skew-symmetric schemes is that they conserve kinetic energy [50]. Now, since this operator is applied to a vector by being applied to each component of that vector, we have

$$S(\vec{u})\vec{u} \approx \vec{u} \cdot \nabla\vec{u}. \tag{2.13}$$

where

$$(S(\vec{u})\vec{u})_\alpha = S(\vec{u})u_\alpha, \tag{2.14}$$

Applying these approximation to the spatial derivatives in the model equations, we have:

$$\rho \left(\frac{\partial \vec{u}}{\partial t} + S(\vec{u})\vec{u} \right) + \vec{D}p = \mu L \vec{u} + \vec{f}, \tag{2.15}$$

$$\vec{D} \cdot \vec{u} = 0, \tag{2.16}$$

$$\vec{f}(\vec{x}, t) = \sum_{k=0}^{N-1} \vec{F}(k\Delta s, t)\delta_h(\vec{x} - \vec{X}(k\Delta s, t))\Delta s, \tag{2.17}$$

$$\frac{\partial \vec{X}}{\partial t}(k\Delta s, t) = \sum_{\vec{x}} \vec{u}(\vec{x}, t)\delta_h(\vec{x} - \vec{X}(k\Delta s, t))h^2, \tag{2.18}$$

where equation (2.18) sums over all points in the support of the delta function. This delta function in the spreading/interpolation steps is replaced with a regularized (or smoothed) approximation:

$$\delta_h(\vec{x}) = \frac{1}{h^2}\phi\left(\frac{x}{h}\right)\phi\left(\frac{y}{h}\right), \tag{2.19}$$

where h is the fluid grid spacing and

$$\phi(r) = \begin{cases} \frac{1}{4}\left(1 + \cos\left(\frac{\pi r}{2}\right)\right), & |r| \leq 2, \\ 0, & \text{otherwise,} \end{cases} \tag{2.20}$$

where r is a dimensionless spatial coordinate [43]. This regularized delta function has compact support and was the approximation in the original IBM proposed by Peskin. Note that the sums in (2.17) and (2.18) are performed only over those points ($k\Delta s$ and $\vec{x}$ respectively) that lie within the support of the discrete delta function. Since then, improved delta regularizations have been derived that yield improved accuracy in the smoothing and interpolation steps, such as the following [28]:

$$\phi(r) = \begin{cases} \frac{1}{8}(3 - 2|r| + \sqrt{1 + 4|r| - 4|r|^2}), & |r| \leq 1, \\ \frac{1}{8}(5 - 2|r| + \sqrt{-7 + 12|r| - 4|r|^2}), & 1 \leq |r| \leq 2, \\ 0, & \text{otherwise,} \end{cases} \tag{2.21}$$

which is the approximation we use in our numerical simulations.

2.2 Temporal discretization

For the temporal discretization of equations (2.15)-(2.18), Peskin uses a second order accurate Runge-Kutta scheme based on the midpoint rule [43], where we have

$$\frac{u^{n+\frac{1}{2}} - u^n}{\Delta t/2} = f(u^n), \tag{2.22}$$

$$\frac{u^{n+1} - u^n}{\Delta t} = f(u^{n+\frac{1}{2}}). \tag{2.23}$$

This scheme incorporates a mixture of forward and backward Euler for the first substep $(n \to n + \frac{1}{2})$, which is first-order accurate. Then, for the next substep, $(n + \frac{1}{2} \to n + 1)$, the scheme uses a combination of midpoint rule and trapezoidal rule (for the viscous term) result in a second-accurate scheme. The temporal discretization is designed in a way that improves the numerical stability by handling terms implicitly wherever possible, while keeping the discrete equations linear.

Applying this scheme to the current method, the forces and positions for IB grids are updated to the half time step $t_{n+1/2}$. Using this data, the velocity at the half time-step is calculated. Using all this information from the half-time step, the final velocity is calculated at the next time step t_{n+1}. In summary, the solution update for velocity and pressure proceeds in two half time steps as follows:

- Solve for $\vec{u}^{n+\frac{1}{2}}$ and $\tilde{p}^{n+\frac{1}{2}}$:

$$\begin{cases} \rho \left(\dfrac{\vec{u}^{n+\frac{1}{2}} - \vec{u}^n}{\Delta t/2} + S(\vec{u}^n)\vec{u}^n \right) + \vec{D}\tilde{p}^{n+\frac{1}{2}} = \mu L \vec{u}^{n+\frac{1}{2}} + \vec{f}^{n+\frac{1}{2}}, \\ \vec{D} \cdot \vec{u}^{n+\frac{1}{2}} = 0, \end{cases} \tag{2.24}$$

where $\tilde{p}^{n+\frac{1}{2}}$ is not the physical pressure but rather plays the role of a Lagrange multiplier that calculates $\vec{u}^{n+\frac{1}{2}}$ to satisfy the discrete incompressibility condition. The position of the IB points is updated similarly using the velocity at the half time-step.

- Solve for $\vec{u}^{n+1}$ and $p^{n+\frac{1}{2}}$:

$$\begin{cases} \rho \left(\dfrac{\vec{u}^{n+1} - \vec{u}^n}{\Delta t} + S(\vec{u}^{n+\frac{1}{2}})\vec{u}^{n+\frac{1}{2}} \right) + \vec{D}p^{n+\frac{1}{2}} = \mu L \left(\dfrac{\vec{u}^n + \vec{u}^{n+1}}{2} \right) + \vec{f}^{n+\frac{1}{2}}, \\ \vec{D} \cdot \vec{u}^{n+1} = 0. \end{cases} \tag{2.25}$$

where $p^{n+\frac{1}{2}}$ is again another Lagrange multiplier for calculating the velocity at the end of time-step and is not the actual pressure.

In both substeps, after rearranging the equations, we need to solve linear systems of the form

$$\begin{cases} \left(1 - \dfrac{\Delta t}{2} \dfrac{\mu}{\rho} L \right) \vec{u} + \dfrac{\Delta t}{\rho} \vec{D}q = \vec{w}, \\ \vec{D} \cdot \vec{u} = 0. \end{cases} \tag{2.26}$$

where $\vec{w}$ is a vector of known values and we have to solve for $\vec{u}$ and q.

For the first half time-step $(n \to n + \frac{1}{2})$ we have:

$$\vec{u} = \vec{u}^{n+\frac{1}{2}}, \quad q = \frac{1}{2}\tilde{p}^{n+\frac{1}{2}}$$

$$\vec{w} = \vec{u}^n - \frac{\Delta t}{2} S(\vec{u}^n) \vec{u}^n + \frac{\Delta t}{2\rho} \vec{f}^{n+\frac{1}{2}}$$

and for the second half time-step $(n + \frac{1}{2} \to n + 1)$:

$$\vec{u} = \vec{u}^{n+1}, \quad q = \frac{1}{2} p^{n+\frac{1}{2}}$$

$$\vec{w} = \vec{u}^n - \Delta t S(\vec{u}^{n+\frac{1}{2}}) \vec{u}^{n+\frac{1}{2}} + \frac{\Delta t}{\rho} \vec{f}^{n+\frac{1}{2}} + \frac{\Delta t}{2} \frac{\mu}{\rho} L \vec{u}^n$$

Finally, the linear system in equation (2.26) can be solved using the discrete Fourier transform (DFT) since the equations now have constant coefficients due to their linearization and the domain is square with periodic boundary conditions. Now by applying DFT to the linear system, we will end up with the following equations:

$$\left(1 - \frac{\Delta t}{2} \frac{\mu}{\rho} \hat{L} \right) \hat{\vec{u}} + \frac{\Delta t}{\rho} \hat{\vec{D}} \hat{q} = \hat{\vec{w}}, \tag{2.27a}$$

$$\hat{\vec{D}} \cdot \hat{\vec{u}} = 0. \tag{2.27b}$$

Now if we apply $\hat{\vec{D}}\cdot$ to the first equation (2.26a), all terms with a factor of $\hat{\vec{D}} \cdot \hat{\vec{u}}$ will be equal to zero. Thus, the first equation reduces to an expression for $\hat{q}$ in terms of $\hat{w}$ only. Next, by rearranging the final equation, we can obtain $\hat{q}$ as

$$\hat{q} = \frac{\hat{\vec{D}} \cdot \hat{\vec{w}}}{\frac{\Delta t}{\rho} \hat{\vec{D}} \cdot \hat{\vec{D}}}, \tag{2.28}$$

and then $\hat{\vec{u}}$ is

$$\hat{\vec{u}} = \frac{\hat{\vec{w}} - \frac{\hat{\vec{D}} \hat{\vec{D}} \cdot \hat{\vec{w}}}{\hat{\vec{D}} \cdot \hat{\vec{D}}}}{1 - \frac{\Delta t}{2} \frac{\mu}{\rho} \hat{L}}, \tag{2.29}$$

Here, the DFT diagonalizes the linear system. So in Fourier space, the denominator in both (2.28) and (2.29) is simply a constant which greatly simplifies the calculation of $\hat{q}$ and $\hat{u}$. Finally, the pressure and velocity will be found by applying the inverse DFT to the transformed unknowns $\hat{q}$ and $\hat{\vec{u}}$ [44]. In most immersed boundary implementations, the DFT is calculated using the fast Fourier transform (FFT).

One other important point about this scheme is that analytically, the pressure Poisson equation with periodic boundary conditions is only determined up to a constant; so the solution is not unique. In terms of the DFT variable $\hat{q}$, this introduces an arbitrary shift between solutions values on even and odd numbered grids, which results in an oscillatory behavior in pressure. However, these oscillations don't affect $\hat{u}$ because the $\hat{\vec{D}} \cdot \hat{q}$ operator eliminates the constant shift.

2.3 IBM algorithm summary

The numerical scheme described in the last section is designed in a way to obtain second-order accuracy in time and space for problems that have smooth solutions. Based on this numerical scheme, for solving an IBM problem, the following algorithm should be applied:

- Compute the force density $\vec{F}^n(s,t)$ on the immersed boundary from the current boundary configuration, $\vec{X}^n$.

- By equation (2.3), calculate the effect of these deformation forces from the Lagrangian nodes to the adjacent fluid grid points.

- Solve the Navier-Stokes equations (2.1) and (2.2) on the Eulerian domain and update $\vec{u}^{n+1}$ and $\vec{p}^{n+1}$ form $\vec{u}^n$ and $\vec{p}^n$.

- Update the location of the Lagrangian points on the IB, $\vec{X}^{n+1}$, using the local fluid velocities, $\vec{u}^{n+1}$ and equation (2.4).

We will apply this algorithm as implemented in the open-source IB2d software package [7], for which a description will be provided in the next chapter.

Chapter 3

Cochlea model and IB2d implementation

3.1 Cochlear physiology

The ear is the organ in the body that is responsible for hearing and is divided into three major sections: outer ear, middle ear and inner ear. Each section has evolved to perform a specific function in the hearing process. Sound waves are oscillations in air pressure which enter the outer ear and travel down the ear canal, which channels and amplifies the waves until they reach the eardrum or tympanic membrane as shown in Figure 3.1. These vibrations are then transferred to a series of three bones or ossicles within the middle ear that further amplify the vibrations. The third and final bone (called the stapes) is connected to another membrane called the oval window, which transfers the sound waves to the cochlea or inner ear. The purpose of the cochlea is to transform these vibrations into electrical nerve impulses that are transmitted to the brain and recognized as individual sound frequencies. [10, 1].

The cochlea is a spiral-wound cavity located in the inner ear that is filled with fluid. As pictured in Figure 3.2, this organ is divided into three liquid-filled chambers: the scala vestibuli, the scala media, and the scala tympani. The first two chambers are separated by Reissner's membrane (RM), which is very flexible. The scala media and the scala tympani are separated by a structure called the cochlear partition (CP). The CP mainly consists of an elastic membrane known as the basilar membrane (BM), which has a variable elastic stiffness that decreases along its length, from base to apex. Two other important structures that sit on the BM are called the tectoral membrane and the Organ of Corti, the latter which contains the mechano-sensitive hair cells that are the main sensory receptors in the ear.

As mentioned before, in the process of hearing, the primary function of the cochlea is to convert the vibrations entering the inner ear into electrical nerve impulses. When these vibrations enter the cochlea through the stapes, they excite the fluid in the cochlear duct.
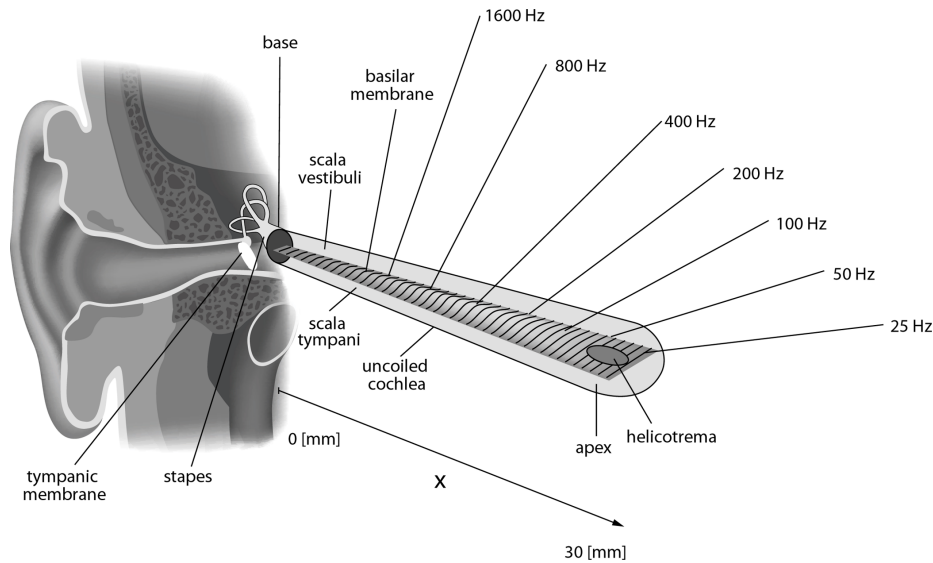
Figure 3.1: Diagram showing the structure of the human ear. Sound travels down the hearing canal to the tympanic membrane, which are then transferred by the bony stapes to the oval window (at the base), which then enters the cochlea (inner ear). The cochlea and basilar membrane are depicted here as unrolled to illustrate the location of peak amplitudes for different sound frequencies. Source: [25, Figure 2] (CC BY 4.0).

This excitation causes the formation of a pressure wave which then travels through the fluid along the basilar membrane from base to apex, deflecting the BM. The deflection of the basilar membrane then stimulates the hair cells due to the motion of the Organ of Corti. These hair cells are tuned to respond to different sound waves based on their frequencies [13]. High-frequency waves stimulate the hair cells closer to the base while low-frequency waves stimulate the ones closer to the apex as shown in Figure 3.1. This is known as cochlear tuning. When the hair cells detect the frequency they are sensitive to, they generate electrical impulses which then travel along the auditory nerves to the hearing centers in the brain [13].

3.2   Mathematical models of the cochlea

Mathematical models for the cochlea can be divided into two categories: passive and active models [54]. In the passive models, the sensory processing in the cochlea is assumed to have two separate steps. In the first step, the peak "place" for each frequency is defined by the interaction of the BM and the fluid. Then, the Organ of Corti and its frequency-sensitive hair cells perform a further sharpening and amplification.

The first type of passive models assumed the ear to be a group of tuned resonant cavities. The first famous resonance theory was introduced by Helmholtz in 1875 [60]. He developed a model in which the BM is made of a set of resonating fibres under tension, acting like the strings in a piano. The fibres close to the base are stimulated by high frequency sounds while
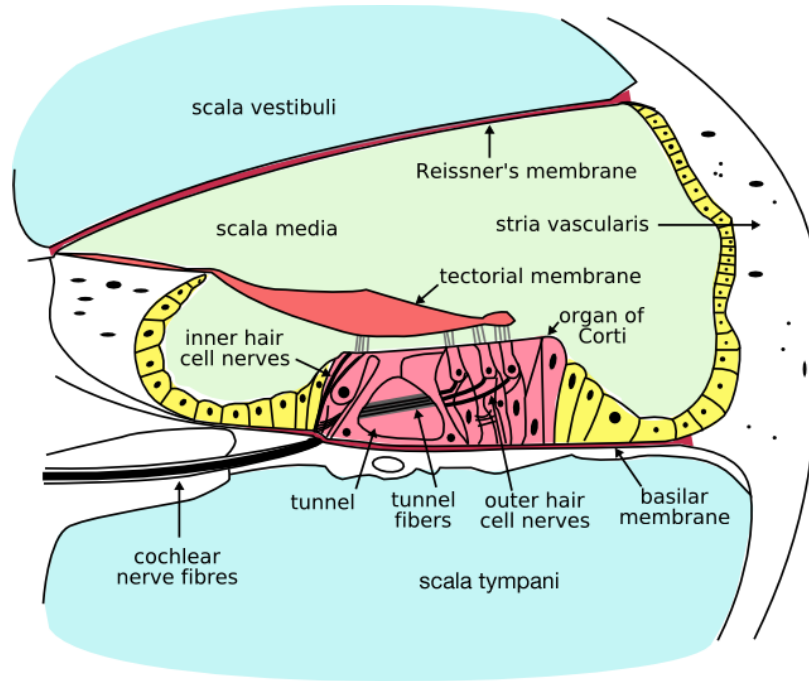
Figure 3.2: Diagram showing the cross-section of cochlea. Source: [62] (CC BY-SA 3.0).

the ones near the apex respond to low frequencies. This feature is called the place principle. However, a major defect in Helmholtz's theory is that it requires the BM to operate under a very high tension, which is not actually observed in experiments.

The next class of passive models was developed by von Békésy [59] in 1928 and is known as the travelling wave theory. Von Békésy observed travelling waves along the cochlea in human and animal cadavers. In his experiments, a place principle still holds, meaning that the peak still migrates further from the base as the frequency decreases, but the amplitude is not very localized in this theory. Also, von Békésy's model simplifies the cochlea greatly by reducing it to a straight tube containing only the BM. Nonetheless, travelling wave models have been the prevailing approach used to understand how the cochlea works. Initially, the models based on traveling wave theory assumed that the fluid motion is one-dimensional [53], which introduces some physically undesirable side-effects for several reasons. First, they assume that BM has a significant mass which was in contrast with von Békésy's observations that the BM mass is negligible in comparison with the surrounding fluid and the significant mass is mainly from the fluid. In addition, different measurements illustrated dispersive effects within the cochlea that are incompatible with the simple 1D traveling wave approximation [33].

The next class of passive cochlea models, incorporating a 2D fluid motion, was introduced by Ranke [47] where he mentioned that 1D non-dispersive models are not consistent with the experimental data. After that, several 2D models were introduced where the BM is assumed to be built out of a collection of damped mass-spring systems and the fluid dy-

namics are simplified to a linear potential flow [3, 29, 38]. A couple of years later, Steele [22] provided a thorough analysis of 2D fluid motion without any a priori assumption of long or short wavelengths. In all these models, an external forcing that is a given sinusoidal function of time is applied to the BM, as the effect of sound waves on the stapes motion. Pozrikidis [45] replaced this forcing with a point source at the stapes and a point sink at the round window and solved the model using a boundary integral method. All of these 2D models allow the assumption of a mass-less partition (BM) which better approximates the physiological properties of the BM.

To more accurately reproduce the behavior observed in experiments, some works developed 3D models which include the component of fluid motion in the transverse direction across the basilar membrane [46, 9, 27] As shown by [55, 41], the 3D fluid dynamic effects have a significant influence on the pressure distributions within the cochlear duct.

In contrast with passive models, the second class of active models attempt to capture the experimental observation that BM vibrations appear to induce a compressive nonlinearity. This provides a positive feedback locally along the CP, which results in higher sensitivity and frequency selectivity. This is often referred to as the cochlear "active process". Gold [19] was the first person to recognize this active process and suggest that some active mechanism might play an important role in cochlear mechanics. This was also seen in the measurements of Rhode [52] who recognized that a significant degree of nonlinearity exists in the BM where the maximum amplitude occurs. Kemp [24] discussed that sound pulses entering the ear can result in echoes generated by the cochlea that are delayed relative to the source signal (called "tinnitus"), meaning that the ear itself can generate sound. Many active models have since been introduced that incorporate the electromotility of the outer hair cells, which is their ability to contract or elongate due to changes in the intracellular potential, and its feedback into the BM [14, 16, 56]. Experimental measurements have confirmed that damaged or dead cochleas exhibit a response similar to that of passive models whereas normal cochleas must generate some active forcing that cannot be captured using passive models. More recent efforts in cochlea modelling combine von Békésy's travelling wave theory and some active cochlear process to better understand how cochlear mechanics contributes to sound sensation [40, 48, 5].

The immersed boundary method has been exploited in different works to provide a realistic model of the fluid dynamics in the cochlea and the interactions between the fluid and basilar membrane. First, LeVeque et al. [30, 31] developed an IB model of the cochlea in which the elasticity of the BM is approximated using simple springs and the fluid obeys the unsteady Stokes equation. Their papers derived an asymptotic solution for traveling waves along the BM. A couple of years later, Beyer [8] provided a cochlea model in which the fluid obeys the full Navier-Stokes equation, including the nonlinear term. He also performed numerical simulations of his model and showed that his results are consistent with the asymptotic solution provided by LeVeque et al. for low frequencies. In all these models,

cochlea is assumed to be a straight, rectangular duct. While this approximation has a small effect on fluid dynamics [17], in the apical region of the BM which is densely coiled, the effect of cochlea curvature cannot be neglected [35]. A 3D IBM model of cochlea has also been developed to represent a more detailed cochlea geometry [18].

3.3 Our cochlea model

Here we consider a simple 2D model, as illustrated in Figure 3.3, which is developed based on the model that Beyer [8] introduced. In our model, the cochlear duct is treated as a rectangular strip $\Omega = [0.5, 4.5] \times [0.5, 2]$ and a 3.5 cm BM lies in the middle of this rectangle, which is the actual cochlea length in humans. In this model, the walls of the cochlear duct are assumed to be rigid structures while the BM is treated as an elastic structure. The stapes is the location where the waves enter the cochlear duct, travel along the BM from the base to the apex, enter the lower channel and finally exit from the round window. The stapes and round window are assumed to have the same cross-sectional area.

Different assumptions and simplifications have been made to reduce the complexity of this problem, while keeping the key elements of the cochlea. A very common simplification is that the spiral coiled cochlea is approximated with a straight tube. Different works discussed that this simplification only has a slight impact on the BM motion [57, 59]. Next, the structural components of the Organ of Corti in the CP are often neglected and only the BM is included. The three channels of cochlea will also be reduced to two channels, the scala vestibuli and the scala tympani by ignoring the very flexible Reissner's membrane (RM). This assumption is valid since the RM has shown to have little impact on the BM and fluid motion [21, 34]. The fluid in the cochlea is assumed to be incompressible and the BM mass is neglected. According to von Békésy's observations [59] that cochlea tuning did not happen when the fluid was drained from the ear, the BM resonance as the mechanism for this tuning is eliminated which justifies neglecting the inertial effects.

In the 3D straight tube representation of the cochlea, as shown in Figure 3.1, the BM is depicted as a narrow plate which is fixed at its edges in the transverse (out of plane) direction. To represent this structure in 2D, we assume this narrow plate is made of a set of disconnected beam elements, with stiffness that acts only in the radial (y) direction. It has been discussed by Allen and Sondhi [2] that excluding the longitudinal stiffness gives better results in comparison with experiments. The coupling of each of these beams to its edge is shown in the 2D model as a restoring force that is independent at each point along the BM. The magnitude of this force depends on the BM stiffness at that point. According to von Békésy's experiments [59], the stiffness of the BM beam elements (represented as points in 2D) has the following form:

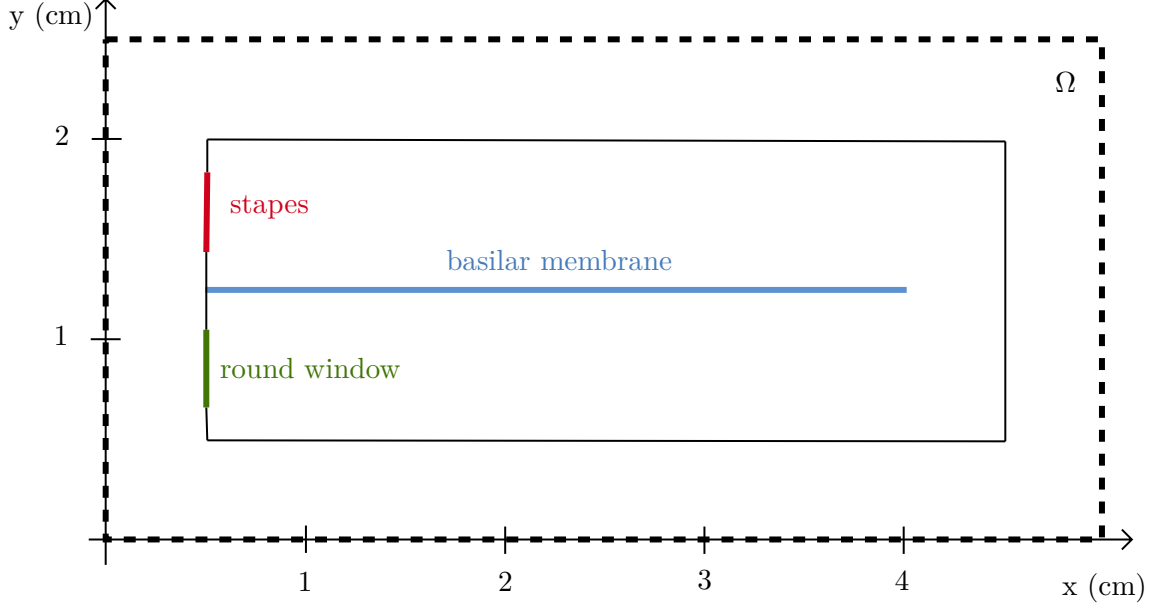$$K(x) = S_0 e^{-\lambda(x-0.5)} \tag{3.1}$$

Figure 3.3: Geometry of the 2D immersed boundary model for the cochlea. The dashed line represents the fluid domain Ω.

where S_0 and λ are positive constants which is different in humans and animals, and $(x-0.5)$ represents the distance from the base along the BM. As it was mentioned, stiffness decreases along the BM from base to apex.

Based on the mentioned assumptions and simplifications, the 2D IB model of the cochlea can be described as follows:

$$\rho\left(\frac{\partial u}{\partial t} + \vec{u} \cdot \nabla \vec{u}\right) + \nabla p = \mu \Delta \vec{u} + \vec{f}, \tag{3.2}$$

$$\nabla \cdot \vec{u} = 0 \quad \text{for } \vec{x}, \tag{3.3}$$

$$\frac{\partial \vec{X}}{\partial t}(s,t) = \int_\Omega \vec{u}(\vec{x},t)\delta(\vec{x} - \vec{X}(s))d\vec{x}, \tag{3.4}$$

where the fluid equations are solved for $x \in \Omega = [0,5] \times [0,2.5]$, which fully encloses the cochlear duct. Here, the elastic force imposed on the fluid by the basilar membrane is given by

$$\vec{f}(\vec{x},t) = \int_0^{3.5} K(s)(\vec{X}_0 - \vec{X})\delta(\vec{x} - \vec{X}(s))ds, \tag{3.5}$$

where $\vec{X}(s,t)$ is the position of the BM, $s \in [0,3.5]$ is the Lagrangian coordinate (equal to distance along the BM), $\vec{X}_0 = [x,1.25]$ is the rest state of the BM and the stiffness is given as

$$K(s) = S_0 e^{-\lambda s} \tag{3.6}$$

16

Variable	Value
Fluid viscosity (μ)	$0.01 \text{ g cm}^{-1} \text{s}^{-1}$
Fluid density (ρ)	1 g cm^{-3}
Elastic stiffness decay rate(λ)	1.4 cm^{-1}
Elastic stiffness (S_0)	$1 \times 10^6 \text{ g cm}^{-2} \text{s}^{-2}$
Forcing frequency (ω)	$[31.25, \ 250] \text{ s}^{-1}$
Forcing amplitude ($U_{\max}$)	0.05 cm s^{-1}

Table 3.1: Physical parameter values in cgs units from [31, 8] for human cochlea.

where S_0 is the elastic stiffness constant and the exponent λ captures the exponential rate of decrease for the BM stiffness along its length.

In this setting, the external force imposed on the fluid boundary is caused by the sinusoidal fluid velocity imposed at the stapes, which has the following form:

$$\vec{U}_{flow}(0.5, y, t) = [U_{max} \left(1 - \cos(2\pi\omega t)\right), 0] \qquad \text{for} \quad 1.4375 \leq y \leq 1.8125. \qquad (3.7)$$

where U_{max} is a constant and ω is the frequency of the entering wave. Due to conservation of mass, eventually fluid will exit the round window with the negative of this velocity. This target velocity is imposed by applying a penalty force at points along the stapes as described in the next section. The no-slip condition on the solid walls of the cochlear duct is imposed by using IB points that are connected to stationary target points with a very large spring stiffness, $K_s = 10^7 \text{dyne/cm}^3$.

This cochlea model incorporates a number of physical parameters that should be defined. In the experiments by von Békésy [59], he observed that in a human cochlea, the BM stiffness at the apex is almost two orders of magnitude smaller than the stiffness at the base. Based on his observations, von Békésy proposed the value for decay rate of stiffness to be $\lambda \approx 1.4 \text{ cm}^{-1}$. The perilymph fluid in the inner ear has a density and viscosity almost equal to that of water. These and other physical parameters are taken from the papers [8, 31] which we use to compare our simulation results with. All these parameters that are used in our model are listed in Table 3.1. All parameter are from Beyer' paper [8] except for U_{max} which is scaled by 5 as he reports this value in a nondimensional setting.

3.4 IB2d framework

The IB2d package [7] uses the IBM scheme discussed in chapter 2 to solve FSI problems. For the fluid solver section, this package assumes that periodic boundary conditions are imposed on all sides of the rectangular fluid domain. the fluid domain. For the immersed boundary part of the model, IB2d provides a wide range of different fiber models that can be assigned to the boundary points in order to represent the desired material properties for

different applications. Based on the chosen fiber model, the total deformation energy of the BM can be calculated by adding the energy of all fiber models that are used:

$$E(\vec{X}(s,t),t) = \sum_{k=0}^{M} E_k\left(\vec{X}_{k,1}, \vec{X}_{k,2}, \ldots, \vec{X}_{k,N}\right) \tag{3.8}$$

where $\vec{X}(s,t)$ is the location of immersed boundary points, N is the number of Lagrangian points and M represents the number of fiber models used to model the immersed boundary. After calculating the deformation energy, the elastic force of the the boundary points is derived as

$$\vec{\mathbb{F}}_{k,c}\left(\vec{X}(s,t),t\right) = -\frac{\partial E(\vec{X}(s,t),t)}{\partial \vec{X}_{k,c}} \tag{3.9}$$

where k represent the fiber model and c is the Lagrangian point for which the force is being calculated. The negative sign comes from the restoring behavior of the force, meaning that this force will drive the system towards a minimal energy state. Finally, the forces from all fibers are added together at each point on the immersed boundary using equation (2.6).

The different fiber models available for use in IB2d are summarized below:

- Target points: boundary points that have a preferred position or motion are defined using a target point model. In this fiber model, each of these immersed boundary points are assumed to be connected to a virtual point via a stiff spring with a resting length equal to zero. The motion of these target points are then controlled by their respective virtual point and the stiffness of the spring that connects the two points.

- Springs: when the elastic structure requires resistance to changing the distance between each successive pair of Lagrangian points, the fiber connecting these two points is modeled using Hookean or non-Hookean springs with resting length R_L and spring stiffness k_s.

- Torsional springs (beams): When the immersed boundary requires resistance to bending, it can be modeled using this fiber model. Here, the model assumes a desired angle θ and a recommended curvature between three successive Lagrangian points and a bending stiffness of k_B which restores the the structure to its resting form to model the desired property.

- Massive points: The approach in this fiber model is that the massive points do not directly interact with the fluid flow, but they act as virtual points connected to the Lagrangian points of the IB. When the IB points move due to fluid motion, they move away from their respective massive points. This will cause a restoring force to move the massive points closer to the IB points.

- Porosity: If the model requires permeability of the immersed boundary, this fiber model would be a good choice since it allows fluid to flow through the immersed structure.

- Muscle-fluid-structure model: A simple muscle model which incorporates both force-velocity and length-tension relationships in the muscle. In this model, the underlying cellular processes of the muscles are excluded from the model and only the mechanical behavior of the muscle is incorporated.

Based on these definitions, the potential energy and elastic force for each fiber model can be computed. Our cochlea model uses only the target point model, for which the energy calculation is discussed next.

The elastic potential energy for target points is

$$E_{target} = \frac{1}{2}k_T||\vec{X}_M - \vec{X}_M^T||^2 \tag{3.10}$$

where k_T is the target point stiffness, $\vec{X}_M$ is the position of physical target points and $\vec{X}_M^T$ is the coordinate of their respective virtual points. The corresponding elastic force at target points is

$$\vec{F}_{target} = -\frac{\partial E_{target}}{\partial \vec{X}_M} = -k_T \begin{pmatrix} x_M - x_M^T \\ y_M - y_M^T \end{pmatrix} \tag{3.11}$$

When the target point force model is being used to mimic a solid rigid boundary then the stiffness constant k_T should be chosen very large so that IB points do not deviate very far from their target locations.

In the IB2d package, besides the various possible fiber models used to handle different types of immersed boundaries, it is also possible to add a couple of other physical features, such as an additional body force term in the fluid equations (gravity, for example) or tracer points that move with the fluid velocity without affecting the fluid motion. One other IB forcing type that is particularly useful for our cochlea model is a penalty force that is used to impose a target velocity at certain locations in the flow, such as the stapes velocity along the oval window described in the previous section. This force acts as a penalty term that is added to the external forcing term in the Navier-Stokes equations of the fluid motion. Here, we define a desired velocity profile $\vec{U}_{flow}(\vec{x}, t)$ on a subset of Eulerian fluid grid points and a force will be imposed on these fluid grid points due to deviation of their velocity from this desired profile. This penalty force has a form similar to that of the spring force for Lagrangian points, but is instead imposed on velocities as:

$$\vec{F}_{arb} = k_{arb}\left(\vec{u}(\vec{x}, t) - \vec{U}_{flow}(\vec{x}, t)\right) \tag{3.12}$$

where k_{arb} is the penalty-strength coefficient, which is an artificial parameter that is simply chosen large enough so that the target velocity is approximately attained during the simulation.

IB2d is a Matlab and Python implementation of the fluid and immersed boundary forcing scheme described above. Here, we will explain the IB2d work flow in the MATLAB implementation. When setting up a model in IB2d, first all the chosen parameters of the model are defined in a file called *input2d*. Then the geometry of the immersed structure and the fiber models associated to its Lagrangian points are implemented in a MATLAB script under the name of the structure, e.g. *cochlea.m*. By running this file, the IB geometry is constructed in a collection of data files and all the fiber models will be assigned to their corresponding nodes. Next, the simulation is started by calling the *main2d* function. This function reads all the information from *input2d* and pass them to the *IBM_Driver.m* function, where the spatial and temporal discretization of IBM is implemented and the model will be simulated there. When the simulation is finished, the structure of the updated IB will be saved along with any other desired properties as a series of .vtk files which can be visualized using different software like ParaView or VisIt.

IB2d provides a comprehensive and integrated environment for simulating IBM problems, but there exist some restrictions that may cause trouble while working with this package. First, it is only accurate for problems with Reynolds number in the range $[0.01, 1000]$. It is also restricted to 2D models where the incompressible flow assumption for the fluid is valid. For the fluid domain with grid dimensions exceeding 512×512 points, the computational cost can become too excessive for normal desktop computers.

3.5   Implementation of cochlea in IB2d

We next describe the IB2d implementation of our cochlea model described in section 3.3, for which the cochlea geometry is shown in Figure 3.4. First, the physical parameters used in this implementation (Table 3.1) are defined in the *input2d* file. In the same file, the rectangular fluid domain for this problem is chosen to be $[0, 5] \times [0, 2.5]$ in order to contain the entire cochlear duct and also capture the fluid motion in and out of the oval and round windows. The fluid mesh size and time-step are also defined in *input2d*. Next, the geometry of the cochlear duct is constructed in *cochlea.m* as a rectangular duct with rigid walls and an elastic membrane in the middle to represent the BM. The stapes and the round window are defined as two holes where the sinusoidal forcing is imposed on the fluid grid points of the hole representing the stapes. The rigid walls making up the outer boundaries of the cochlear duct are defined as target points with large stiffness of $k_T = 10^7 \ gcm^{-2}s^{-2}$. Because of this large stiffness, the motion of these points is very tightly restricted and so they behave collectively as if they approximate a rigid, stationary wall.
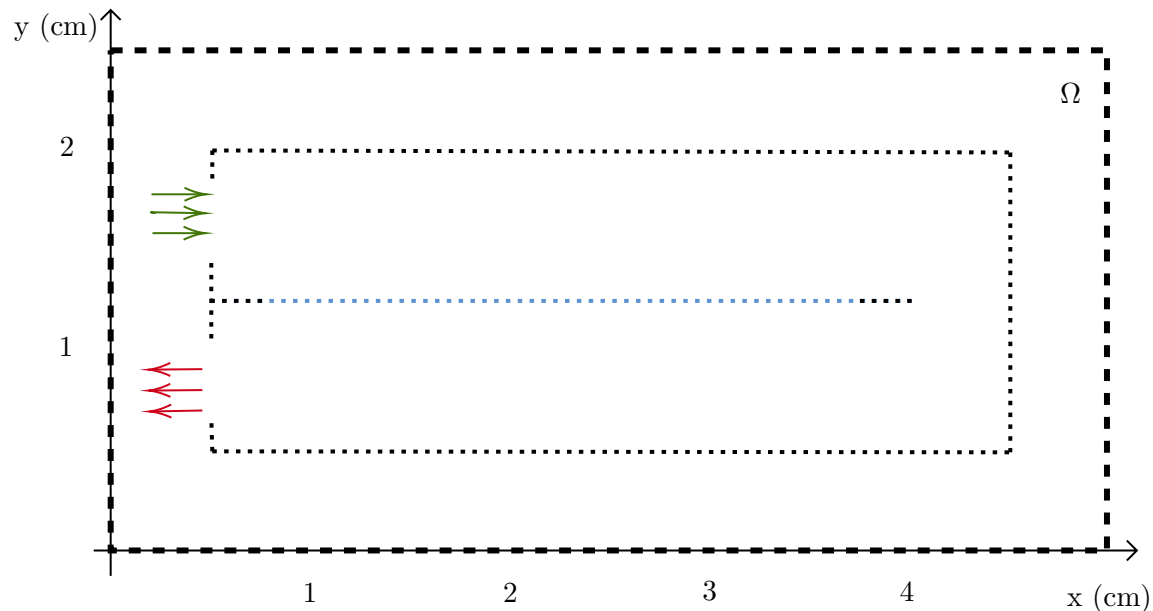
Figure 3.4: IB2d implementation of the cochlea: black nodes represent rigid target points, blue nodes show elastic target points along the BM with varying stiffness. The green arrows represent the fluid velocity $\vec{U}_{flow}$ at the oval window driven by the stapes, and the red arrows depict the corresponding velocity $-\vec{U}_{flow}$ at the round window.

For modelling the basilar membrane, its Lagrangian points are assumed to be target points as well, but with a smaller stiffness that decreases along the BM from base to apex. Here, due to smaller stiffness of target points,the flows induced by the imposed stapes motion is sufficient to cause these points to move. In this 2D model of the cochlea, virtual points associated with the BM target points represent the fixed edges of the deflected beams in the BM plate in 3D. Since the BM plate has a solid connection at its basal and apical ends, 10 Lagrangian points at each end of the BM are assumed to be rigid adjacent to the base and apex.

After defining this cochlear duct geometry in *cochlea.m*, the external forcing is implemented in a separate function called *please_Compute_External_Forcing.m*. The target velocity function is defined based on equation (3.7) and is used to impose this external force at each fluid grid point lying along the stapes.

In the next chapter, we perform a number of numerical simulations using this IB model and compare with other asymptotic and numerical results.

Chapter 4

Numerical simulations

In this chapter, we will present numerical simulations of the cochlea model described in Chapter 3 for different frequencies of the external forcing corresponding to the input sound signal and compare the results with other numerical and asymptotic results.

The physical parameters are based on the values from Table 3.1. The time step has been set as $\Delta t = 0.51 \times 10^{-4}$ s, since for the fluid mesh size that we have, the scheme will be stable. In the forcing function, the penalty-strength coefficient is $k_{arb} = 10^3$. To ensure that the ends of the BM are anchored and to minimize nonphysical oscillations near the endpoints, 10 nodes at each end of this membrane are treated as fixed target points with a large stiffness equal to that for the target points making up the cochlear duct. When modelling the cochlea, many physical and computational parameters combine together to affect the cochlear tuning. Choosing these parameters in order to achieve the tuning that we expect from cochlea is quite a challenge, since a small change in one parameter may result in unusual behaviour or an imperfectly tuned basilar membrane oscillations. In this work, different parameters have been tested from various works in order to determine the values that produce the closest fit with experimentally observed BM behaviour.

Our first simulation uses a forcing frequency of $\omega = 125$ Hz on a 256×256 fluid grid. The result is shown in Figure 4.1. The maximum amplitude at each point along the BM is shown as upper (or lower) "envelope curves", that represent the maximum (or minimum) extent over time of the BM displacement reached at every point. In other words, all BM displacement curves for a given simulation are bounded between the upper and lower envelope curves. The raw max/min values computed from the IB2d simulation data are shown as two curves in the figure. A smoother envelope function is then computed, based on a least-squares cubic spline fit through the tangent points based on the algorithm introduced by McClain *et al.* [36], that is plotted as a black curve in this figure. This smoother curve helps with eliminating the noisy, high-frequency features to better understand the BM behavior.

As expected, this input frequency excites an oscillation that has a peak or local maximum in the amplitude at a distinct location along the BM called the "place", which for this frequency is at a BM location of roughly 2 cm. Based on the behavior of the cochlea, we
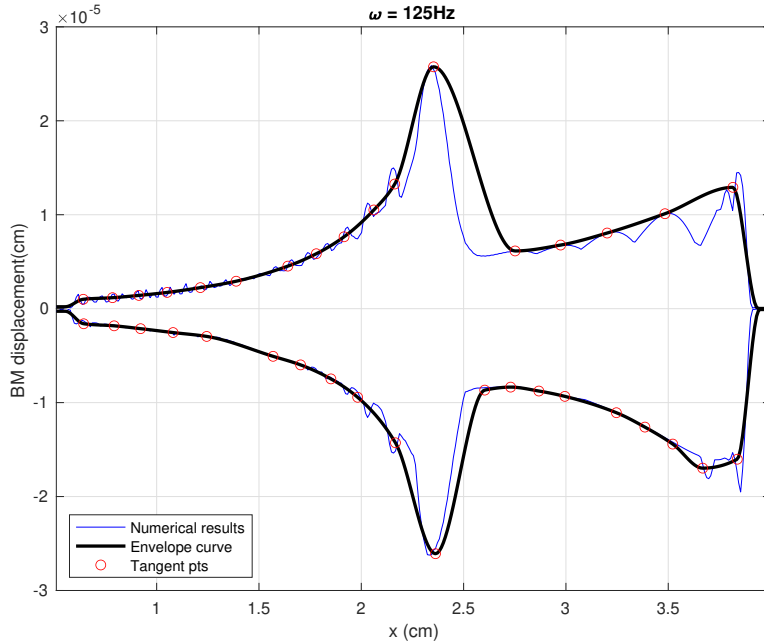
Figure 4.1: BM envelope curves for forcing frequency $\omega = 125\text{Hz}$ on 256×256 fluid domain.

expect that when the envelope curve reaches its peak, the amplitude damps out quickly. What we see here, which is not consistent with our expectations, is the increase in amplitude at the apical end of the BM, which we call an "end bump". The cochlear tuning works in a way that after the peak location for each frequency, the fluid viscosity damps out the wave and the amplitude of this wave will decay rapidly. However, due to the lower stiffness of the points after the peak location, if even a small part of this wave survives, we will not observe the decaying amplitude. This means that a balance between the cochlear stiffness and the fluid viscosity is required for the system to be perfectly tuned. Different factors can can disrupt this expected cochlear tuning. One scenario that could cause this odd behavior is the simplifications and assumptions that we made to develop the model. There may exist some physics that are not incorporated into the model, which cause the end bump to happen. We have gone through most of these changes to obtain more accurate results, but there may be some that we missed. One other scenario might be the geometry of our cochlea model. The actual cochlea is a is a tapered duct that decreases in height from base to apex and which might cause the pressure waves to die out more rapidly towards the apex. So, in the rectangular geometry that we picked, the waves possibly do not vanish as fast as they should. Another possible cause is the BM stiffness function, which in our model only depends on the distance from the base along the BM. This function is only an approximation of the actual stiffness and there may be other parameters effecting this stiffness that are not captured by this function.

Other than this end bump, the peak location for this frequency occurs near the middle of the BM roughly 2 cm from the base, which is consistent with Beyer's result for this frequency [8, Figure 7] after converting his dimensionless plot to dimensional variables. The amplitude of this peak is also in the range of both physically measured amplitudes (which are on the order of 10's of nm) [59] and other numerical simulations [39].

The velocity field for this simulation is illustrated in Figure 4.2 at the final time. According to this figure, the fluid behavior is what we would expect at an instant in time when the stapes is deforming the oval window inwards. The fluid is forced towards the right along the basilar membrane and makes a turn at the apical gap or helicotrema. The flow then continues to the left along the lower duct where it ultimately causes the membrane at the round window to deform outwards. Near the peak location (pictured in the bottom plot of Figure 4.2) we can see a circular motion of the fluid near the point of maximum amplitude. This is also consistent with Beyer's results depicted in [8, Figure 6]. Note that despite the velocity vectors pointing inward at the stapes (oval window) and outward at the round window, there is no fluid flowing into or out of the cochlear duct; instead, our IB model captures the effects of the solid deformable membranes that cover the two window openings.

In Figure 4.3 the same configuration has been solved on a 512×512 fluid grid. As we can see, the peak location occurs almost at the same place as what we saw in Figure 4.1 and the maximum amplitude has the same order, despite the different behavior of the plots at the right end. By comparing the two results, we observe that the solution appears to be relatively independent of mesh size at this resolution. So for the remaining simulations, we will use a 256×256 fluid grid. The results of these simulations for different frequencies are depicted in Figure 4.4.

In order to validate the results with other methods, other than showing that the peak amplitude has the same order of magnitude with other works, a useful comparison is provided by the plot of BM peak location versus forcing frequency. For this purpose, the local maximum of the BM amplitude at the peak location is plotted for seven frequencies in the range $[31.25, 250]$ Hz in Figure 4.5. This figure shows that, as frequency increases, not only the peak location keeps getting closer to the base at the beginning of the BM but also the amplitude of this peak keeps getting smaller. Most importantly, there is a clear linear dependence between the peak location and the logarithm of the forcing frequency. This behavior is also consistent with the results from LeVeque *et al.* [31, Figure 2], where the peak location is calculated using the following asymptotic formula [31]

$$x_p = \frac{1}{4\lambda} \log\left(\frac{S_0^4 \lambda^2}{8\rho^3 \mu}\right) - \frac{7}{4\lambda} \log(\omega), \tag{4.1}$$
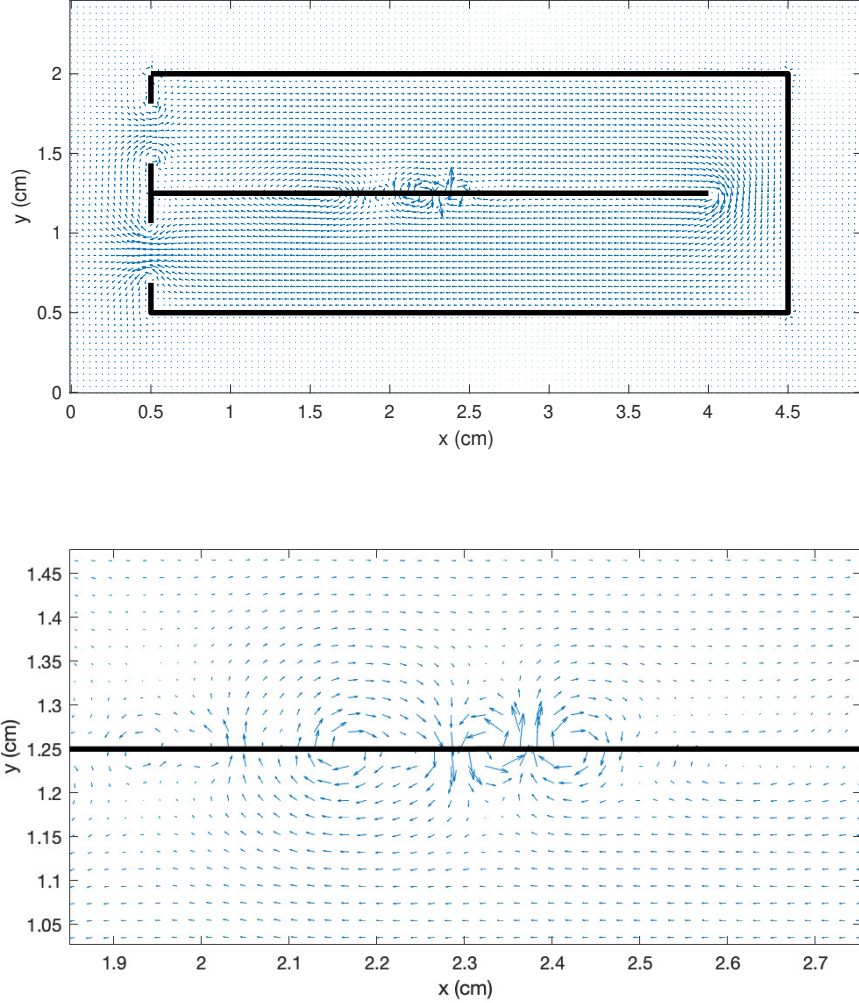
where ω is the forcing frequency.

24

Figure 4.2: Velocity field forcing frequency $\omega = 125$Hz on 256×256 fluid domain. Bottom figure shows a zoomed in picture at peak location.

According to [8, Figure 8], Beyer also reports an increasingly oscillatory behavior of the envelope curve for higher frequencies. This shows that he also observe some odd behavior for frequencies beyond 250 Hz. This may be the reason that he restricted his study to frequencies in the range [31.25, 250]Hz, while the actual range of frequencies that human can hear is much wider, from 20 Hz to 20 kHz. Figure 4.5 also includes a comparison of the peak BM locations along with an asymptotic solution derived by LeVeque *et al.* [31], which shows the our results are consistent with the asymptotic solution. Since Beyer [8] presented his results in terms of a normalized BM amplitude, it is not possible to make a direct comparison of amplitude, but qualitatively, our work is consistent with his. In addition, since he verified his results with the asymptotic solution provided by LeVeque *et al.* [31] as
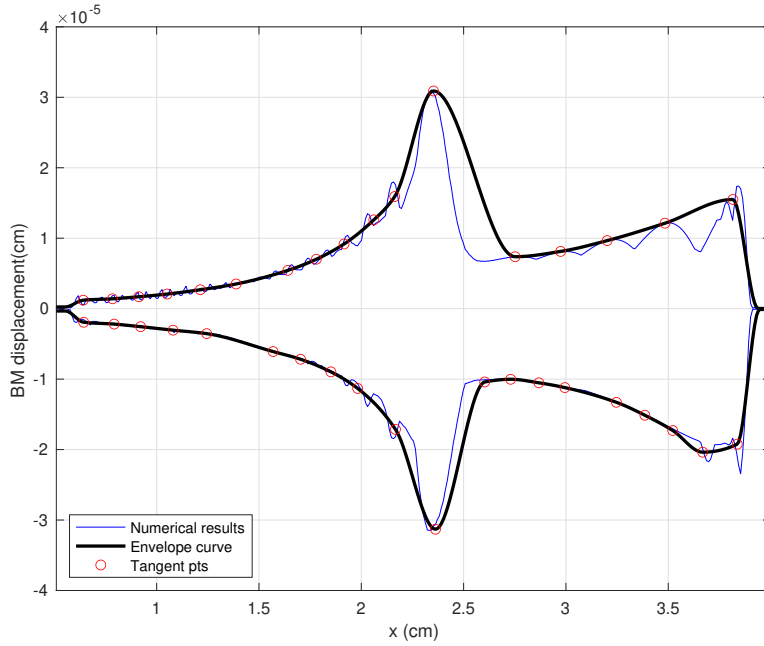
Figure 4.3: BM envelope curves for forcing frequency $\omega = 125$Hz on 512×512 fluid domain.

well, it is safe to say that our work is consistent with Beyer's [8]. The asymptotic solution of LeVeque *et al.* [31] is also verified with experimental data provided by von Békésy [59].

In Figure 4.6, we can easily see the decaying behavior of peak amplitude for higher frequencies, where the amplitude is also roughly proportional to $\log(\omega)$. This is also consistent with the results in [31, Figure 3].
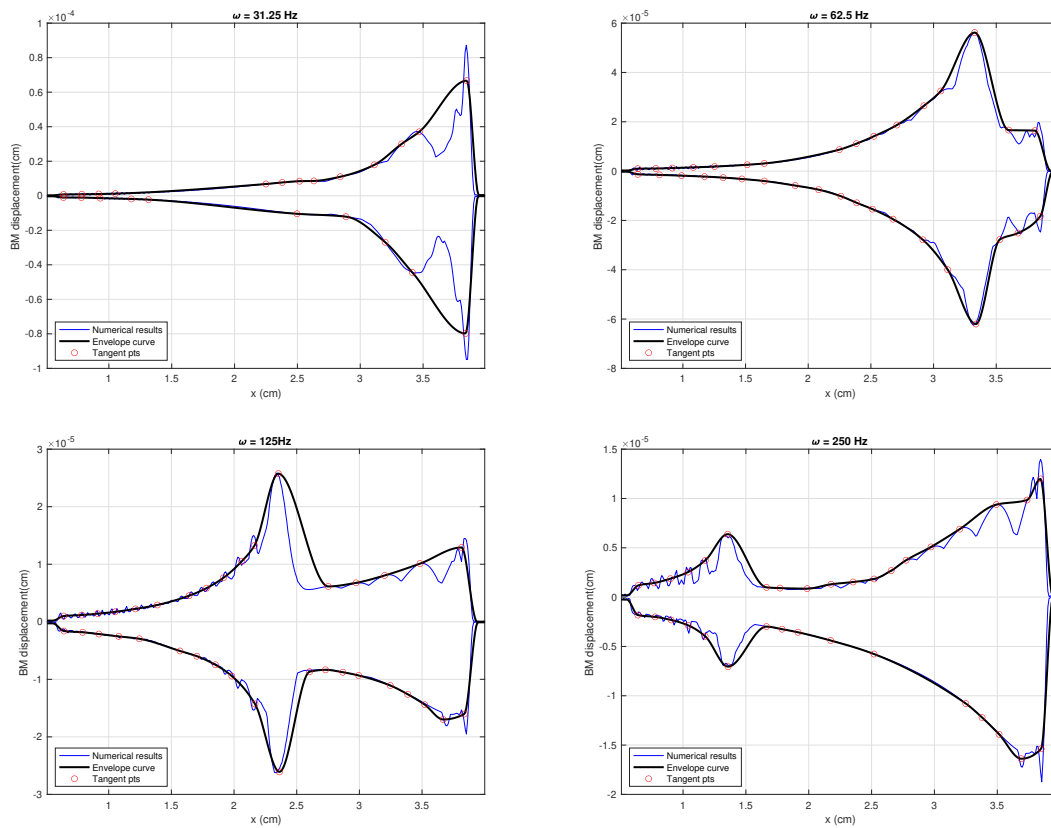
Figure 4.4: BM envelope curves for different forcing frequencies. The peak location moves towards the base as frequency increases.
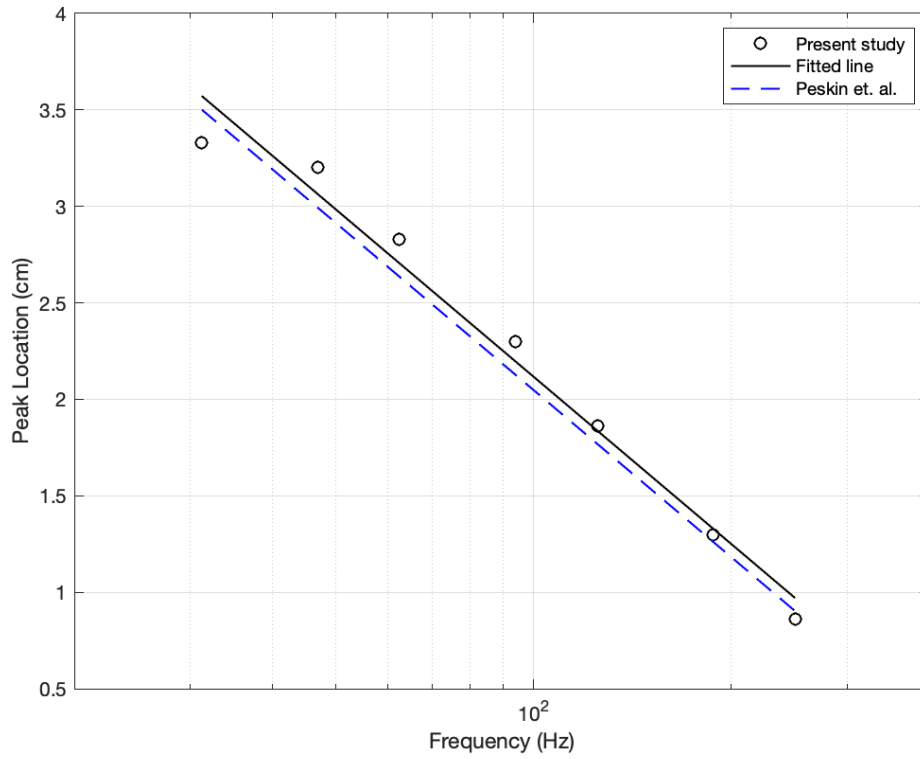
Figure 4.5: Peak location as a function of stapes frequency compared with the asymptotic solution provided by LeVeque *et al.* [31].
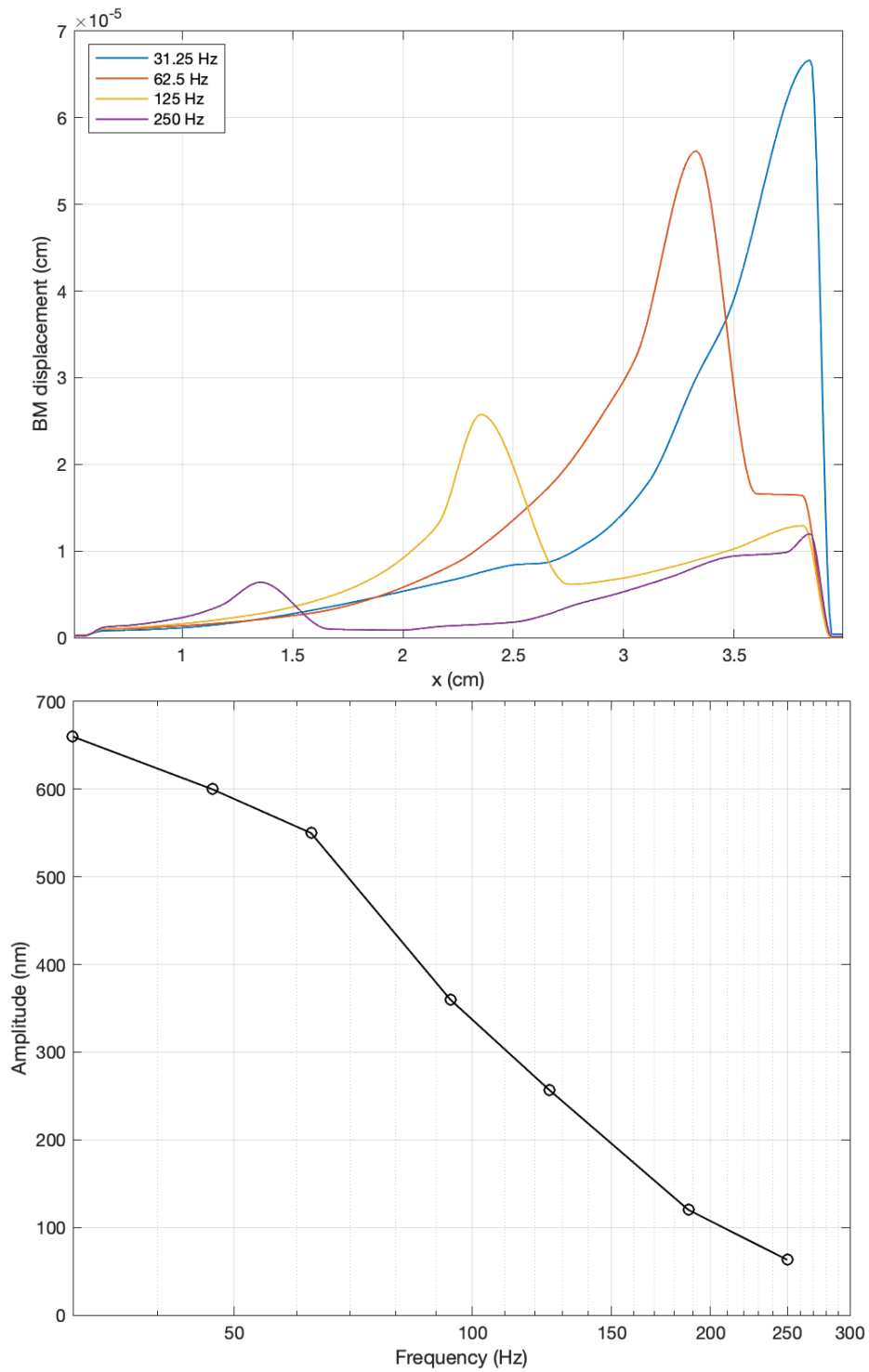
Figure 4.6: Upper envelope curve for different frequencies is shown in the top plot. Bottom plot depicts the exponential decay of the peak amplitude with respect to frequency increase.

Chapter 5

Conclusion

In this thesis, we presented a 2D IB model of the cochlea using the immersed boundary method developed by Peskin [43]. In this model, we approximated the cochlea to be a rectangular duct with the basilar membrane located in the middle. This model is then implemented in IB2d [7], which is a package for the 2D simulation of immersed boundary problems. Simulation results for different frequencies are then presented, showing that the peak locations corresponding to these frequencies and their peak amplitudes are consistent with other works. We also observe the well-established result that the peak amplitude decreases at a rate that is roughly proportional to $-\log \omega$, where ω is the forcing frequency. However, there exists an "end bump" at the apical end the BM which is not consistent with the observed behavior of BM where the fluid motion should be more rapidly damped out after the peak location due to viscous effects. Various reasons such as the geometry of the model or the chosen stiffness function, have been discussed for the occurrence of this end bump.

After the "end bump" issue has been resolved, this IB model for the cochlea provides an excellent platform for further investigations of cochlear mechanics. One extension that can be included is the Reissner's membrane, which is a spatially uniform elastic structure that is much less stiff than the BM and has been connected with otoacoustic emissions from the inner ear [49]. It would also be interesting to incorporate other aspects of the cochlea structure such as the frequency-sensitive hair cells that are embedded within the BM and Organ of Corti.

Bibliography

[1] AglaSem Schools. Ncert book, class 11 biology, chapter 21: Neural control and coordination. `https://schools.aglasem.com/ncert-books-class-11-biology-chapter-21`.

[2] J. Allen and M. Sondhi. Cochlear macromechanics: Time domain solutions. *Journal of the Acoustical Society of America*, 66(1):123–132, 1979.

[3] J. B. Allen. Two-dimensional cochlear fluid model: New results. *Journal of the Acoustical Society of America*, 61(1):110–119, 1977.

[4] J. B. Allen and S. T. Neely. Micromechanical models of the cochlea. *Physics Today*, 45(7):40–47, 1992.

[5] J. Ashmore, P. Avan, W. E. Brownell, P. Dallos, K. Dierkes, R. Fettiplace, K. Grosh, C. M. Hackney, A. J. Hudspeth, F. Jülicher, et al. The remarkable cochlear amplifier. *Hearing Research*, 266(1-2):1–17, 2010.

[6] N. A. Battista, W. C. Strickland, A. Barrett, and L. A. Miller. IB2d reloaded: A more powerful Python and Matlab implementation of the immersed boundary method. *Mathematical Methods in the Applied Sciences*, 41(18):8455–8480, 2018.

[7] N. A. Battista, W. C. Strickland, and L. A. Miller. IB2d: a Python and MATLAB implementation of the immersed boundary method. *Bioinspiration & Biomimetics*, 12(3):036003, 2017.

[8] R. P. Beyer Jr. A computational model of the cochlea using the immersed boundary method. *Journal of Computational Physics*, 98(1):145–162, 1992.

[9] F. Böhnke, J. Mikusch-Buchberg, and W. Arnold. 3D finite elemente Modell des cochleären Verstärkers. *Biomedizinische Technik*, 42(s2):311–312, 1997.

[10] J. Casale, P. F. Kandle, I. Murray, et al. Physiology, cochlear function. StatPearls Publishing, `https://www.ncbi.nlm.nih.gov/books/NBK531483`. Accessed on March 18, 2022.

[11] A. Champneys, D. Avitabile, M. Homer, and R. Szalai. The mechanics of hearing: a comparative case study in bio-mathematical modelling. *The ANZIAM Journal*, 52(3):225–249, 2011.

[12] R. Cortez, L. Fauci, N. Cowen, and R. Dillon. Simulation of swimming organisms: Coupling internal mechanics with external fluid dynamics. *Computing in Science & Engineering*, 6(3):38–45, 2004.

[13] P. Dallos. The active cochlea. *Journal of Neuroscience*, 12(12):4575–4585, 1992.

[14] E. de Boer. Auditory physics.Physical principles in hearing theory. III. *Physics Reports*, 203(3):125–231, 1991.

[15] D. J. Eyre and A. L. Fogelson. IBIS: A software system for immersed boundary and interface simulations. `http://www.math.utah.edu/IBIS`, 1997.

[16] C. D. Geisler. A realizable cochlear model using feedback from motile outer hair cells. *Hearing Research*, 68(2):253–262, 1993.

[17] C. D. Geisler. *From sound to synapse: physiology of the mammalian ear.* Oxford University Press, USA, 1998.

[18] E. Givelberg and J. Bunn. A comprehensive three-dimensional model of the cochlea. *Journal of Computational Physics*, 191(2):377–391, 2003.

[19] T. Gold. Hearing. II. The physical basis of the action of the cochlea. *Proceedings of the Royal Society of London. Series B–Biological Sciences*, 135(881):492–498, 1948.

[20] B. E. Griffith. IBAMR: An adaptive and distributed-memory parallel implementation of the immersed boundary (IB) method. `https://github.com/IBAMR/IBAMR`, 2014.

[21] A. Inselberg and R. S. Chadwick. Mathematical model of the cochlea. I: formulation and solution. *SIAM Journal on Applied Mathematics*, 30(1):149–163, 1976.

[22] D. H. Jen and C. R. Steele. Electrokinetic model of cochlear hair cell motility. *Journal of the Acoustical Society of America*, 82(5):1667–1678, 1987.

[23] J. Keener and J. Sneyd. The inner ear. In *Mathematical Physiology*, volume 8 of *Interdisciplinary Applied Mathematics*, chapter 23, pages 701–728. Springer-Verlag, New York, 1998.

[24] D. T. Kemp. Stimulated acoustic emissions from within the human auditory system. *Journal of the Acoustical Society of America*, 64(5):1386–1391, 1978.

[25] A. Kern, C. Heid, W.-H. Steeb, N. Stoop, and R. Stoop. Biophysical parameters modification could overcome essential hearing gaps. *PLoS Computational Biology*, 4(8):e1000161, 2008.

[26] C. Kleinstreuer. *Biofluid Dynamics: Principles and Selected Applications.* CRC Press, Boca Raton, FL, 2006.

[27] P. J. Kolston and J. F. Ashmore. Finite element micromechanical modeling of the cochlea in three dimensions. *Journal of the Acoustical Society of America*, 99(1):455–467, 1996.

[28] M.-C. Lai and C. S. Peskin. An immersed boundary method with formal second-order accuracy and reduced numerical viscosity. *Journal of Computational Physics*, 160(2):705–719, 2000.

[29] M. B. Lesser and D. A. Berkley. Fluid mechanics of the cochlea. Part 1. *Journal of Fluid Mechanics*, 51(3):497–512, 1972.

[30] R. J. LeVeque, C. S. Peskin, and P. D. Lax. Solution of a two-dimensional cochlea model using transform techniques. *SIAM Journal on Applied Mathematics*, 45(3):450–464, 1985.

[31] R. J. LeVeque, C. S. Peskin, and P. D. Lax. Solution of a two-dimensional cochlea model with fluid viscosity. *SIAM Journal on Applied Mathematics*, 48(1):191–213, 1988.

[32] M. J. Lighthill. *Mathematical Biofluiddynamics*. Society for Industrial and Applied Mathematics, Philadelphia, PA, 1975.

[33] S. J. Lighthill. Biomechanics of Hearing Sensitivity. *Journal of Vibration and Acoustics*, 113(1):1–13, 1991.

[34] D. Manoussaki and R. S. Chadwick. Effects of geometry on fluid loading in a coiled cochlea. *SIAM Journal on Applied Mathematics*, 61(2):369–386, 2000.

[35] D. Manoussaki, E. Dimitriadis, and R. Chadwick. Cochlea's graded curvature effect on low frequency waves. *Physical Review Letters*, 96(8):088701, 2006.

[36] M. McClain, A. Feldman, D. Kahaner, and X. Ying. An algorithm and computer program for the calculation of envelope curves. *Computers in Physics*, 5(1):45–48, 1991.

[37] O. Mesnard. pyIBM: an immersed boundary method python code. `https://github.com/mesnardo/pyIBM`, 2014.

[38] S. T. Neely. Finite difference solution of a two-dimensional mathematical model of the cochlea. *Journal of the Acoustical Society of America*, 69(5):1386–1393, 1981.

[39] G. Ni, S. J. Elliott, and J. Baumgart. Finite-element model of the active organ of Corti. *Journal of the Royal Society Interface*, 13(115):20150913, 2016.

[40] R. Nobili, F. Mammano, and J. Ashmore. How well do we understand the cochlea? *Trends in Neurosciences*, 21(4):159–167, 1998.

[41] E. S. Olson. Observing middle and inner ear mechanics with novel intracochlear pressure sensors. *Journal of the Acoustical Society of America*, 103(6):3445–3463, 1998.

[42] C. S. Peskin. Flow patterns around heart valves: A numerical method. *Journal of Computational Physics*, 10(2):252–271, 1972.

[43] C. S. Peskin. The immersed boundary method. *Acta Numerica*, 11:479–517, 2002.

[44] C. S. Peskin. Lectures on the immersed boundary method. Courant Institute, New York University, `https://www.math.nyu.edu/~peskin/ib_lecture_notes/`, 2007.

[45] C. Pozrikidis. Boundary-integral modeling of cochlear hydrodynamics. *Journal of Fluids and Structures*, 24(3):336–365, 2008.

[46] M. N. Raftenberg. Flow of endolymph in the inner spiral sulcus and the subtectorial space. *Journal of the Acoustical Society of America*, 87(6):2606–2620, 1990.

[47] O. F. Ranke. Theory of operation of the cochlea: A contribution to the hydrodynamics of the cochlea. *Journal of the Acoustical Society of America*, 22(6):772–777, 1950.

[48] T. Reichenbach and A. J. Hudspeth. The physics of hearing: Fluid mechanics and the active process of the inner ear. *Reports on Progress in Physics*, 77(7):076601, 2014.

[49] T. Reichenbach, A. Stefanovic, F. Nin, and A. J. Hudspeth. Waves on Reissner's membrane: A mechanism for the propagation of otoacoustic emissions from the cochlea. *Cell Reports*, 1(4):374–384, 2012.

[50] J. Reiss. A family of energy stable, skew-symmetric finite difference schemes on collocated grids. *Journal of Scientific Computing*, 65(2):821–838, 2015.

[51] K. A. Rejniak. An immersed boundary framework for modelling the growth of individual cells: An application to the early tumour development. *Journal of Theoretical Biology*, 247(1):186–204, 2007.

[52] W. S. Rhode. Observations of the vibration of the basilar membrane in squirrel monkeys using the Mössbauer technique. *Journal of the Acoustical Society of America*, 49(4B):1218–1231, 1971.

[53] W. M. Siebert. Ranke revisited – A simple short-wave cochlear model. *Journal of the Acoustical Society of America*, 56(2):594–600, 1974.

[54] C. R. Steele, G. J. Baker, J. A. Tolomeo, and D. E. Zetes-Tolomeo. Cochlear mechanics. In *Biomedical Engineering Fundamentals*, pages 1147–1162. CRC Press, 2006.

[55] C. R. Steele and L. A. Taber. Comparison of WKB calculations and experimental results for three-dimensional cochlear models. *Journal of the Acoustical Society of America*, 65(4):1007–1018, 1979.

[56] S. Verhulst, T. Dau, and C. A. Shera. Nonlinear time-domain cochlear model for transient stimulation and human otoacoustic emission. *Journal of the Acoustical Society of America*, 132(6):3842–3848, 2012.

[57] M. A. Viergever. Basilar membrane motion in a spiral-shaped cochlea. *Journal of the Acoustical Society of America*, 64(4):1048–1053, 1978.

[58] G. von Békésy. Zur Theorie des Hörens: Die Schwingungsform der Basilarmembran. *Physikalische Zeitschrift*, 29(22):793–810, 1928.

[59] G. Von Békésy and E. G. Wever. *Experiments in Hearing*. McGraw-Hill New York, 1960.

[60] H. Von Helmholtz. *On the Sensations of Tone as a Physiological Basis for the Theory of Music*. Longmans Green, 1912.

[61] J. Wiens and B. Froese. MatIB: an immersed boundary method package in matlab. `https://github.com/eldila/MatIB`, 2013.

[62] Wikipedia, the free encyclopedia. Cochlea-cross-section. `https://en.wikipedia.org/wiki/File:Cochlea-crosssection.png`, 2004. [The original uploader was Oarih at English Wikipedia].